AD-A114 969 CARNEGIE-MELLON UNIV PITTSBURGH PA ROBOTICS INST F/G 13/9
CONTROL OF A DIRECT-DRIVE ARM,(U)
MAR 82 H ASADA, T KANADE, I TAKEYAMA N00014-81-K-0503
UNCLASSIFIED CMU-RI-TR-82-4 NL

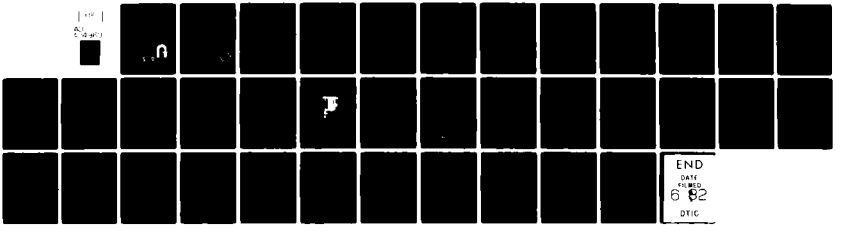

END
DATE FILMED
6 82
DTIC

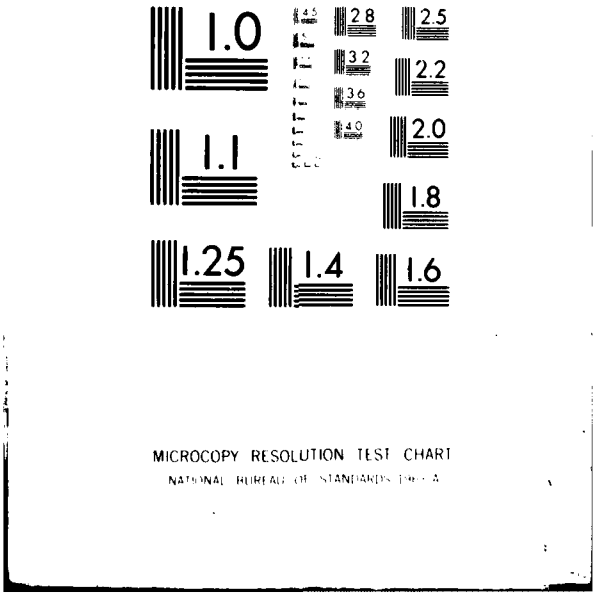
1.0
1.1
1.25
1.4
1.6
1.8
2.0
2.2
2.5
2.8
3.2
3.6
4.0
MICROCOPY RESOLUTION TEST CHART
NATIONAL BUREAU OF STANDARDS 1963-A

(13)

Carnegie-Mellon University

AD A114969

CONTROL OF A DIRECT-DRIVE ARM

Haruhiko Asada
Takeo Kanade
Ichiro Takeyama

The Robotics Institute
Carnegie-Mellon University
Pittsburgh, Pennsylvania 15213

CMU-RI-TR-82-4

THE ROBOTICS INSTITUTE

(13

CONTROL OF A DIRECT-DRIVE ARM

March 9, 1982

Haruhiko Asada
Takeo Kanade
Ichiro Takeyama

Robotics Institute
Carnegie-Mellon University
Pittsburgh, Pennsylvania 15213

[1]This work is supported by The Office of Naval Research (Contract No. N00014-81-K-0503)

Abstract

A direct-drive arm is a new mechanical arm in which the shafts of articulated joints are directly coupled to the rotors of high performance torque motors. Since the arm does not contain any gears or transmission mechanisms between the motors and their loads, the drive systems have no backlash, small friction and high mechanical stiffness, all of which are desirable for fast, accurate and versatile robots. At the Robotics Institute of Carnegie-Mellon University,we have built a first prototype direct-drive arm (referred to as CMU DDArm hereafter). This paper presents the characteristic analysis and the design of the control system. First, we describe an outline of the developed CMU DDArm and compare its characteristics with conventional indirect-drive arms. Second, we discuss basic feedback control for single-link drive systems in the frequency domain. Third, we apply a feedforward compensation to the control of multi-degree-of-freedom motion in order to compensate for interactions among multiple links, and Coriolis, centrifugal and gravitational forces. Finally, the steady-state characteristics are discussed with respect to servo stiffness and positioning accuracy. The experiments show the excellent performance of the direct-drive arm in terms of speed and accuracy. Throughout the paper comparison with indirect-drive methods is made to contrast the advantage of the direct-drive method.

1. Introduction

As robots find more and more advanced application, such as assembly in manufacturing, accurate, fast and versatile manipulation becomes necessary. One of the difficulties in controlling mechanical arms is that they are highly nonlinear and involve coupling among the multiple links. Recent progress in the analysis of arm dynamics allows the real-time computation of full dynamics using efficient algorithms in a recursive Lagrangian formulation [6], a Newton-Euler formulation [10] [13], or a table look-up technique [12]. When an arm is severely loaded or high precision is required , deflections in mechanical components are a significant part of arm dynamics [3]. When arm dynamics are identified accurately, feedforward compensation of nonlinear and interactive torques combined with optimal regulators for the linearized system improves control performance greatly [15], and guarantees a global stability over a wide range of arm configurations.

Critical obstacles to the use of dynamics models lie in the uncertainty of arm dynamics and the difficulty of identification. Even a single component in a drive system, such as a gear, a lead screw, a steel belt, a servovalve or a pipe, has complex and changeable characteristics in terms of friction, deflection, backlash, compressibility and wear. One way to proceed, when arm dynamics are not well identified, is to use model-referenced adaptive control to maintain a uniform performance [5]. Its extensive application has shown to allow decoupling of the arm dynamics in a Cartesian coordinate system [14], the reduction on computational burdens [7], and high speed control [9].

Alternatively, a rather straightforward way to achieve high-quality dynamic performance is to pursue a new mechanism which contains very few uncertain factors. The obedient characteristics of the simplified arm dynamics will make it easy and effective to apply sophisticated control. A direct-drive arm is a new mechanical arm which meets these criteria by radically departing from conventional arm mechanisms. In a direct-drive arm, unlike a conventional mechanical arm that is driven through gears, chains, on lead screws, the joint axes are directly coupled to rotors of high-torque electric motors, and therefore no transmission mechanism is included between the motors and their loads. Because of this, the drive system has excellent features: no backlash, small friction and high stiffness. The authors have developed the first prototype of the direct-drive arm with six degrees of freedom [1] [2]. This simple mechanism allows a clear and precise model of the DDArm dynamics, which is of special importance not only for accurate positioning control but also for compensating interactive and coupling torques in high speed manipulation. This paper describes a characteristics analysis of the direct-drive arm and the design of a control system to achieve the potential for excellent performance that the direct-drive arm presents.

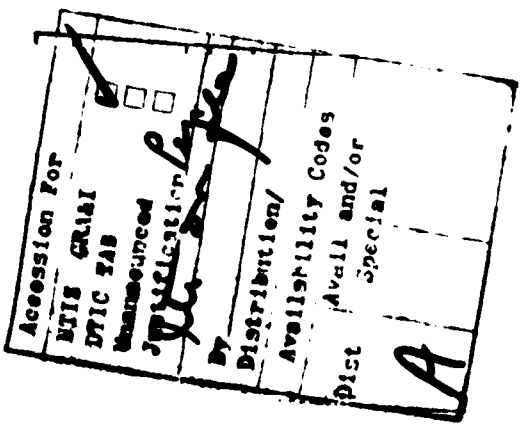

2. Outline of the Direct-Drive Arm

The overall view of the developed DDArm is shown in Photo 1 and its assembly drawing in Figure 1. (The detailed description and data about the CMU DDArm are found in [2]. The arm has 6 degrees of freedom, all of which are articulated direct-drive joints. From the upper base frame, the first joint is a rotational joint about a vertical axis, and the second is a rotational joint about a horizontal axis. The third and fourth joints rotate the forearm about the center axis of the upper arm and about its perpendicular axis, respectively. The fifth and sixth joints perform a rotational and a bending motion of the wrist part. The total length of the arm is 1.7 m, and the movable part from joint 2 to the tip is 1 m. The movable range of joints 1 and 5 is 330 degrees, and the remaining joints can move 180 degrees. The maximum payload is 6kg including a gripper attached at the tip of the arm.

High performance DC torque motors were used for the direct-drive arm. The motor consists of a rotor, a stator and a brush ring. As shown in Figure 1, each component of the motor is installed directly at the joint housing; the rotor on a hollow shaft, and the stator and the brush ring at the case. To develop a torque large enough to rotate the joint shaft directly, we selected motors with large diameters. The motor to drive joint 1 is 56 cm in diameter with 204 Nm peak torque. Joint 2 has two motors, one on each side of the upper arm. These motors are 30 cm in diameter with a total of 136 Nm peak torque. It is required that the motors at joints 4, 5 and 6 have not only high torque but also lightweight and compact size, because heavy motors at these joints give a large load for the upper joints. Therefore we used high performance torque motors with samarium cobalt magnets, whose maximum magnetic energy is 3 to 10 times larger than that of conventional ferrite or alnico magnets. The two samarium cobalt motors to drive joint 4 are 23 cm in diameter with 54 Nm peak torque, and the motors for the last two joints are 8 cm in diameter with 6.8 Nm peak torque.

An optical shaft encoder is installed at each joint to measure the joint angle and its angular velocity. We used precision encoders combined with precision gears with 1 to 4 and 1 to 8 gear ratios. The resultant resolution is 16 bit per revolution for the first 4 joints and 15 bit per revolution for the last 2 joints.

3. Mathematical Modeling and Identification

3.1. Kinematics

We describe the kinematic structure of the arm according to the Denavit and Hartenberg convention [4]. The arm consists of 7 links numbered 0 to 6 from the base to the tip of the arm. Joint i is the joint that connects link $i-1$ to link i.

To represent the geometry, we use coordinate frames attached to each link. Figure 2 shows the disconnected links of the direct-drive arm where the rotors and stators of motors are disassembled and attached to separate links. Table 1 shows the geometry of each link, where

s_i = the distance between x_{i-1} and x_i measured along z_{i-1}.

a_i = the distance between z_{i-1} and z_i measured along x_i, and

α_i = the angle between the z_{i-1} and z_i axes measured in a righthand sense about x_i.

Joint displacement is given by joint angle θ_i that is the angle between the x_{i-1} and x_i axes measured in the righthand sense about z_{i-1}. The above three parameters and one variable completely describe the relation between any adjacent links.

3.2. Arm Dynamics

We derive the equation of motion of the arm assuming that the arm consists of rigid bodies. Motion of a rigid body is decomposed into translation with respect to its center of mass and a rotation about it. Let us denote the translational velocity of a link by a vector v and the angular velocity of rotation by ω respectively. Then the kinetic energy that the link has is given by

$$T_{kinetic} = \frac{1}{2} m v^T v + \frac{1}{2} \omega^T I_{link} \omega \tag{1}$$

where m is the mass of the link, I_{link} is the inertia tensor and ^{T} represents the transpose of a vector. The potential energy of the rigid body is given by

$$U_{potential} = m g^T p^0 \tag{2}$$

where $g^T = (0, 0, g)$ is acceleration vector of gravity and p^0 is the position vector of the center of mass.

The characteristics of a single link is completely represented by mass m, center of mass p, and inertia tensor about the center of mass I_{link}. We computed these parameters for each link of the direct-drive arm from the detail drawings. Table 2 lists the center of mass p and the inertia tensor I_{link} in respect to each link-coordinate frame.

Each body in a series of mechanical links has a constraint in motion due to the linkage. Motion of link i, for example, is related to the movement of preceding joints from 1 to i. Therefore the position, velocity and angular velocity involved in the kinematic energy and potential energy can be represented by joint angles and their derivatives. Combining the energies that all the links have and differentiating with respect to joint angles, the following equation of motion is obtained [11],

$$\tau_i = \sum_{j=1}^{n} J_{ij} \ddot{\theta}_j + \sum_{j=1}^{n} \sum_{k=1}^{n} b_{ijk} \dot{\theta}_j \dot{\theta}_k + fg_i + fd_i \tag{3}$$

τ_i is the torque developed by the motor at joint i. The first term on the right hand side stands for inertia force,

the second term, consisting of products of angular velocities, stands for Coriolis and centrifugal forces, and the third term stands for gravity load. J_{ij} and b_{ijk}, and fg_i depend on the arm configuration, namely θ_1, ..., θ_n. fd_i is the other disturbing torque such as friction and external force. The direct-drive joints have friction only at the bearings that support the joint axes and the brushes between the rotors and stators. This friction is negligibly small for most of the direct-drive joints.

3.3. Drive Systems

A drive sysytem of a joint consists of a motor and a servo amplifier. Since the motor of a direct-drive joint is directly coupled to its joint axis, the driving torque about the axis is exactly the same as the torque developed by the motor, which is proportional to current I_i applied to the motor armature,

$$\tau_i = Kt_i I_i \tag{4}$$

where Kt_i is a torque constant. The electrical characteristics of the armature are given by

$$V_i = R_i I_i + E_i + L_i \frac{dI_i}{dt} \tag{5}$$

where V_i is the applied voltage to the armature of motor i, R_i is resistance of the armature, L_i is its inductance, and E_i is the back EMF. Inductance L_i is negligibly small in most cases. The back EMF is proportional to the angular velocity of joint axis and is given by

$$E_i = Kt_i \dot{\theta}_i \tag{6}$$

where the back EMF constant is the same as the torque constant Kt_i in SI units. The servo amplifier controls the applied voltage V_i to be proportional with its input voltage u_i

$$V_i = Ka_i u_i \tag{7}$$

where Ka_i is the gain of the servo amplifier. The substitution of eqs.(4),(6) and (7) into eq.(5) yields

$$\frac{Ka_i Kt_i}{R_i} u_i = \tau_i + \frac{Kt_i^2}{R_i} \dot{\theta}_i \tag{8}$$

where the inductance L_i is neglected. Thus the drive system is characterized by the following parameters,

$$Ka^*_i = \frac{Ka_i Kt_i}{R_i}$$
$$C_i = \frac{Kt_i^2}{R_i} \tag{9}$$

where Ka^*_i is torque gain between the input u_i and the exerted torque, and C_i represents a damping

coefficient inherent to the drive system. For the arm we have developed joints 2 and 4, each have two motors that work together. We used separate servo amplifiers with a common input u_i. The resultant torque is obtained by summing the torques exerted at each motor driven by the separate amplifiers. The damping torque is also the sum of the damping torque developed at each motor. Therefore the sum of the torque gains and the sum of the damping coefficients give the resultant gain and coefficients. Table 3 shows the parameters identified through experiments.

3.4. Single-Link Model and Frequency Response

As the first step in investigating the characteristics of servomechanisms, we assume a simplified load for each actuator. Namely, we first neglect all the nonlinear effects such as Coriolis and centrifugal forces as well as gravity torque and friction. We also assume that when joint i is investigated all the other joints are mechanically immobilized. Then the equation of motion of the arm is $\tau_i = J_{ii}\ddot{\theta}_i$, because $\ddot{\theta}_j$ and $\dot{\theta}_j$ for $j \neq i$, are all zero. Figure 3 shows the block diagram of the single-link drive system. The blocks enclosed by a broken line represent the control object including a servo amplifier, a motor and the simplified load. The velocity feedback E inside of the control object corresponds to the back EMF of the motor. The equation of the control object is given by

$$u_i = \frac{J_{ii}L_i}{Ka_iKt_i}\dddot{\theta}_i + \frac{J_{ii}R_i}{Ka_iKt_i}\ddot{\theta}_i + \frac{Kt_i}{Ka_i}\dot{\theta}_i \tag{10}$$

We identified the single-link drive systems through experiments. Figures 4, 5 and 6 show the frequency response for joints 1, 4 and 6, which are joints at the shoulder, elbow and wrist of the arm respectively. The inertia load of each joint varies with the arm configuration and payload. Especially, the characteristics of joint 1 vary largely depending on the angle of joint 2. The curves in Figure 4 are Bode diagrams for different arm configurations, $\theta_2 = 0^\circ$, 45° and 90°. In none of the case the phase curve exceeds 180°. Therefore the control object can be identified as a second-order system. It implies that the effect of armature inductance appearing in eq.(10) is negligible. Thus the transfer function of the single-link drive system is given by

$$Go_i(s) = \frac{K_i}{s(T_i s+1)} \tag{11}$$

where time constant T_i and gain K_i are given by

$$T_i = \frac{J_{ii}R_i}{Kt_i^2} = \frac{J_{ii}}{C_i}$$

$$K_i = \frac{Ka_i}{Kt_i} = \frac{Ka^*_i}{C_i} \tag{12}$$

The solid curves in the figures are obtained by an optimal curve fitting to minimize the mean-square

error from the experimental data. The time constant of each joint is then identified and listed in the second column of Table 4.

4. Issues in Controlling the Direct-Drive Arm

Before we design a controller for the direct-drive arm, the characteristics of the direct-drive arm are discussed based on the previous analysis and experiments. We compare the direct-drive arm with a conventional indirect-drive arm that is driven through gears and other means of reducers.

In case of an indirect-drive arm, the torque developed by a motor varies while it is transmitted through the reducer between the motor and its load. If its gear ratio is r, the exerted torque is amplified r times, and some of the resultant torque is spent coping with friction and inertia at the transmission mechanism. The characteristics of transmission mechanisms are rather complicated, but let us assume that its stiffness is virtually infinite and that the mechanisms have no backlash. The net torque to drive the joint axis, in the simplest case, is given by

$$\tau = r\,\mathrm{Kt}\,\mathrm{I} - \mathrm{f_T} - r^2 \mathrm{J_T}\,\ddot{\theta} \tag{13}$$

where $\mathrm{f_T}$ is friction and $\mathrm{J_T}$ is the inertia of transmission mechanism converted at the rotor of motor. The back EMF is also r times larger than that of a direct-drive joint, because the angular velocity of the motor shaft is r times faster than that of the joint axis.

$$\mathrm{E} = r\,\mathrm{Kt}\,\dot{\theta} \tag{14}$$

Substituting eqs. (13) and (14) to eq. (5),

$$r\frac{\mathrm{Ka\,Kt}}{\mathrm{R}}\mathrm{u} = \tau + \mathrm{f_T} + r^2 \mathrm{J_T}\,\ddot{\theta} + r^2\frac{\mathrm{Kt}^2}{\mathrm{R}}\dot{\theta} \tag{15}$$

where the inductance of armature is ignored.

Comparing eq. (8) with eq. (15), we can notice that the transmission of torque from the motor to the load is ideally simple without any disturbance in the case of direct drive. However, we face the following issues in controlling the direct-drive arm.

- **Low damping**

  The damping torque appeared in the last term of eq. (15) is proportional with the square of gear ratio r as well as the squared torque constant. Although the motors used for direct-drive arm have larger motor constants, the direct-drive joint, where the gear ratio is 1, tends to show poor damping characteristics.

  The direct coupling of motors to their loads eliminates friction along with transmission mechanisms. However, since in a indirect coupling Coulomb friction usually opposes the joint

movements and plays a role of the brakes on the joints, the direct coupling also leads to the lower damping than that of indirect-drive joints.

As a matter of fact, the poor damping characteristics are observed in the data of time constants identified through experiments. Because the time constant of the open-loop control system stands for the ratio of inertia J_{ii} to damping coefficient C_i, the large time constants in Table 4 imply that the damping of the direct-drive joints is relatively small to the inertial loads. Therefore we need a means to increase the damping and reduce the time constant in order to stabilize the system.

- **Nonlinearity and interaction**

The direct-drive arm can move very fast because of small friction and no reduction of speed. When the arm moves, the more complicated become the arm dynamics. Coriolis and centrifugal forces in the second term of eq. (3) are proportional with products of angular velocities. Therefore the high-speed direct-drive arm has significantly large effects resulting from these nonlinear forces.

The elimination of the transmission mechanism in the direct-drive arm makes the effect of interactions among multiple links, the Coriolis and centrifugal forces more prominent in the direct-drive arm dynamics than in the indirect-drive arms. This can be understood by considering the inertia at the actuator of the joint. The total inertia which bears on the rotor of the motor is the sum of the inertia at the transmission J_T and the equivalent inertia of its external load (i.e., links) converted to the motor shaft. When we use a transmission mechanism with gear ratio r, the inertia of the external load J_L becomes J_L/r^2 at the rotor. Thus the total inertia is given by

$$J_{total} = J_T + \frac{J_L(\theta)}{r^2} \tag{16}$$

The gear ratio r can be designed so that the maximum power transfer from the motor to the load is obtained. The maximum power transfer is realized when the equivalent inertia of an external load is equal to that of the rotor inertia; that is,

$$J_T = \frac{J_L(\theta_{typical})}{r^2} \tag{17}$$

Notice that J_T does not change as the arm moves, while J_L varies significantly with the arm configuration. The equality in the equation (17) is designed to hold for typical arm configuration. Therefore, in the case of indirect-drive joint with the optimal gear ratio, about 50 % of the total inertia load does not change. Only the latter half has the complicated characteristics. Thus, the arm dynamics tend to be less sensitive to the change of arm configuration. In contrast, in the case of the direct-drive joint, where $r=1$, the complicated arm dynamics is directly reflected to the actuators. The above arguments suggest that in controlling the direct drive arm, we need to compensate the arm dynamics including all the terms appeared in the equation of motion: Coriolis and centrifugal forces and interaction of the multiple links.

5. Feedback Control

5.1. Velocity Feedback

In this section, we discuss velocity feedback to increase damping of the direct-drive joints. In the case of an indirect-drive joint, velocity is usually measured at the shaft of a motor before the speed is reduced by gears. However, it is rather difficult to do so in a direct-drive joint, because the motor speed is as slow as the link motion. We employed high resolution shaft encoders to measure the slow speed movement of the direct-drive joint. The details of velocity measurement are described in [8].

Figure 3 includes a velocity feedback loop, where Kv is the velocity feedback gain. Let us investigate the upper limit of the velocity feedback gain. As shown in Figure 7, the velocity measurement can not be perfect because of quantization error and dead band near zero speed. The minimum speed detectable by the developed encoder circuits is 2 degrees per second for joints 1 to 4, and 4 degrees per second for joints 5 and 6. The quantization error is 1/128 of full scale for all joints. If the velocity feedback gain is extremely large, it amplifies the error as well as the signal. When a joint rotates near the minimum detectable speed, the velocity signal alternates frequently between zero and the minimum value. This alternating velocity signal gives a large fluctuation of control torque and decreases control accuracy. Figure 8 shows the experiments in slow speed control. We observe that a large gain Kv causes a vibration in motion, while a smooth motion is obtained for gain smaller than a certain value. The third column of Table 4 lists the upper limit of the velocity feedback gain for each joint which is determined through experiments for each joint listed.

Figures 4, 5 and 6 also show frequency responses of joints 1, 4 and 6, respectively, after the velocity feedback compensation is done using the maximum allowable gains. The phase curves show a noticeable lead of phase, about 50 to 60 degrees. By fitting theoretical curves to the experimental data, we can obtain the time constants for the improved response. The time constants of the improved systems are listed in Table 4. The velocity feedback compensation decreases the time constants 6 to 13 times smaller than those without it.

5.2. Gain Adjustment

Now we proceed to the gain adjustment for the improved systems. Figure 3 shows a position control system, where Kp is the position feedback gain to be adjusted.

Since overshoot is usually undesirable in the control of mechanical arms, we adjust the position feedback gain Kp so that the damping factor is between 0.9 and 1. Figure 9 shows the step response for joints 1, 4 and 6: response (a) is overdamped, response (b) is underdamped, and response (c) is critically damped. The responses for the three joints are recorded in the same time scale. The response of joint 1, which has a large inertial load, is relatively slow, while joints 4 and joint 6 have very fast responses. To evaluate the transient response we use delay time T_d and settling time T_s. The delay time is the time required for the step

response to reach 50 % of its final value, and the settling time is the one required before settling within 5 % of the final value. The delay times of joint 4 and 6 are only 57 ms and 82 ms respectively. They show that the direct-drive arm we developed has excellent dynamics. Even joint 1 has a 365 ms delay time, which is fast enough for most applications.

5.3. Limitation of Speed

The direct-drive arm has a very fast response as shown in the previous section. When a large step input is applied to one of the fast joints, the joint may be accelerated to an excessively fast speed for a long distance motion. The excessively fast motion is dangerous and is not desired in some applications. The velocity measurement circuit also has an upper limit of measurable speed. If the joint is accelerated to a speed higher than the upper limit, the velocity feedback signal saturates and provides an insufficient damping to the servo controller. The resultant insufficient damping causes an overshoot. Therefore we need to limit, for safety, the speed within an appropriate range. To avoid the acceleration that exceeds the limit, a brake signal to cancel the acceleration is necessary. The ranges in the curve of Figure 7 toward its ends show modified velocity feedback to apply the brakes. If the speed exceeds the normal operating range, the velocity feedback gain is increased to several times larger than the normal operation range. The maximum value of the velocity feedback signal is large enough to cancel the acceleration signal no matter how fast the speed is. Therefore the speed is limited within the allowable range.

Figure 10 shows the experiments of transient response for a large step input. The left two figures are step responses for joint 4, the right two are for joint 6. The upper two are cases without the limit of speed and the lower two are the cases with the limit. Each figure includes position and velocity curves measured by the encoder. The measured velocity saturates soon after the links begin to move. We determined the maximum allowable speed for joints 1 to 4 to be 180 deg/s, and for joints 5 and 6, 360 deg/s. When the speed limit is not installed (a), we notice that the links are accelerated too fast because of the saturation of the velocity feedback, and that large overshoots appear. On the other hand, by the compensation for velocity measurement saturation (b), the links move within the prescribed speed limits. The responses also settle to the reference input smoothly without overshooting. The effect of compensation is very noticeable.

6. Feedforward Control

6.1. Control Scheme

As we have discussed in the previous section, the multiple-degree-of-freedom motion of an arm includes complicated interactions among links. In this section, we discuss the compensation of interactive torques among multiple links and nonlinear torques such as Coriolis, centrifugal and gravity torques. Feedforward control is effective in compensating for the predictable motions, so long as the characteristics of

the arm are identified accurately. The direct-drive arm has the advantage that the simple structure allows us to have an accurate model of the control object.

By solving the equation of motion inversely, we can compute the torques to drive the arm along a specified trajectory [6] [10]. Let $\theta_{r1}(t)$, $\theta_{r2}(t)$, ..., $\theta_{rn}(t)$ be a trajectory of joint angles. If the trajectory is smooth enough to differentiate up to the second order with respect to time, the torques required to trace the trajectory with the specified speed and acceleration, $\dot{\theta}_{ri}$, $\ddot{\theta}_{ri}$ are derived from eq. (3),

$$\tau_{ri}(\theta_r) = \sum_{j=1}^{n} J_{ij}(\theta_r)\ddot{\theta}_{rj} + \sum_{j,k=1}^{n} b_{ijk}(\theta_r)\dot{\theta}_{rj}\dot{\theta}_{rk} + f_{gi}(\theta_r) + f_{ci}(\dot{\theta}_{ri}) \tag{18}$$

where J_{ij}, b_{ijk} and f_{gi} are functions of θ_{r1}, θ_{r2}, ..., θ_{r6} and f_{ci} is Coulomb friction and viscous friction at brushes and bearings. If the identification of the arm is perfect and no other disturbing torque is applied to it, the arm can move along the specified trajectory with the computed torques. However, as the arm travels for a long time, unavoidable errors can be accumulated, even if the identification error and the disturbances are small. Since the coefficients involved in eq. (18) are valid only when the arm configuration is in the vicinity of the predicted state, θ_{ri}, the computed torques do not make much sense if the actual position of the arm diverges from the specified trajectory. Therefore, we need to keep the state of arm close to the reference trajectory. The feedback controller designed in the previous sections provides a continuous positional error correction from their references. We extend it to a controller that can correct the error of joint angle velocities $\dot{\theta}_i$ from their references $\dot{\theta}_{ri}$, as well as the positional errors. By combining the feedforward control with the feedback control, we can expect that the former provides the gross torques to lead the arm to a given trajectory with no delay and that the latter provides the fine error correction to keep the state of arm close to the reference. Thus the total torque applied to joint i is given by

$$\tau_i = \tau_{ri}(\theta_r) + Kp^*_i(\theta_{ri} - \theta_i) + Kv^*_i(\dot{\theta}_{ri} - \dot{\theta}_i) \tag{19}$$

where Kp^*_i is forward-path gain from the position reference to the torque of motor, as shown in Figure 11, Kv^*_i is the resultant velocity-feedback gain including the inherent damping due to the back EMF of motor and the artificial damping through velocity feedback.

$$Kp^*_i = Ka^*_i Kp_i$$

$$Kv^*_i = C_i + Ka^*_i Kv_i \tag{20}$$

The second term and a part of the third term in eq. (19) have been already implemented in the feedback controller previously designed. What is to be added is to solve the inverse problem of arm dynamics by a computer and to provide the torques $\tau_{ri}(\theta_r)$ and $Kv^*_i\dot{\theta}_{ri}$.

6.2. Experiments

Figure 12 shows the experiment of feedforward compensation for joint 4, where the sinusoidal inputs drawn by dash-and-dot lines were given to the system as reference trajectories and its responses after settling into steady oscillations. Curve (a) shows the case with no compensation, in which significantly large offset and phase lag are observed as well as the reduction of amplitude. Curve (b) shows the case with the compensation of gravity torque, where the offset vanished and the amplitude was enlarged. In the case of (c) where the damping torque and Coulomb friction, $Kv^*_i\dot{\theta}_{ri} + fc_i$, as well as the gravity torque were compensated, a remarkable improvement in phaselag can be seen. When all the arm dynamics were taken into account, the resultant response, curve (d), shows the excellent coincidence with the reference trajectory. We observed the excellent corrrespondence with sinusoidal inputs over wide ranges of frequency and amplitude,provided none of the driving torque, angular velocity and acceleration exceeds their limits.

Figure 13 shows the responses of joints 4 and 6 where sinusoidal reference trajectories were given to them simultaneously. When no feedforward compensation was applied, a noticeable interaction from joint 6 to joint 4 was observed. After the full dynamics of the two joints were compensated through the feedforward control, no significant interaction between them was observed and both trajectories showed excellent coincidence with the references.

7. Evaluation of Steady-State Characteristics

7.1. Positioning Accuracy

In this section we evaluate the developed arm with respect to steady-state errors. Figure 14 summarizes the experiment of positioning accuracy, where the histogram of steady-state positioning errors for a step response is shown. Each histogram is obtained by more than 200 trials of the step response from the same point to the same destination. After settling to a final position, the joint angle was measured by a high resolution encoder. The horizontal line in each figure indicates the error from the destination (0 degree). Means and standard deviations were computed for each joint. To improve positioning accuracy, we implemented phase-lag compensators which increase loop gains 10 times larger in the lower frequencies. While joint 1, in figure (a), had a large offset (2.208 deg.) under no compensation, it is reduced to -0.287 deg., which is a reasonable error when compared to indirect-drive arms. More importantly, the standard deviations indicated in the figure are very small; especially when the phase lag compensation was used, the deviation is only 0.019 deg. The smaller joints, joints 4 and 6, show an especially good positioning performance. The small standard deviations, 0.005 deg. for joint 4 and 0.003 deg. for joint 6, show that the direct-drive arm has a great advantage in terms of accuracy as well as speed. One of the reasons for the excellent repeatability is that it does not contain uncertain factors such as large friction at gears and deflection at chains of the direct-drive arm and other flexible components.

7.2. Servo Stiffness

Although the direct-drive arm has less internal disturbances, it is subject to external disturbances in actual operations. For example, the arm mechanically interacts with environments during manufacturing operations, or when the arm grasps an unknown payload. Since the disturbances are not predictable in most cases, we cannot compensate for them through the feedforward control discussed in the previous section.

We evaluate the sensitivity of the developed arm to external disturbances. Assuming that a disturbing torque f_d is applied to a joint axis as shown in Figure 3, the steady-state error for this system is given by

$$e_{steady} = \frac{f_d}{Kp^*} \tag{21}$$

To evaluate e_{steady} we compute the deflection due to the load applied at the tip of each link. Suppose the link length is l and the disturbing force F_d is applied at the tip. Then $f_d = l F_d$, and the resultant deflection d at the tip of the link is

$$d = l e_{steady} = \frac{l^2 F}{Kp^*} \tag{22}$$

We define the servo stiffness Ks of a single link drive system by the ratio of applied force F_d to the deflection d [11].

$$Ks = \frac{F_d}{d} \tag{23}$$

The servo stiffness for joints 1, 4 and 6 are listed in Table 5. The resultant stiffness under the phase-lag compensation is sufficiently large and comparable to the Stanford Manipulator [11].

8. Conclusion

This paper has presented theories and experiments of controlling the direct-drive arm. After describing the outline of the CMU DDArm, we developed the mathematical model of the direct-drive arm dynamics. From the comparison with indirect-drive methods, the advantages of the direct-drive arm in dynamics became clear. The elimination of factors which are uncertain and hard to identify, such as friction, makes it possible to develop a precise mathematical model of arm dynamics and to employ it in arm control. At the same time, the modeling enabled us to identify important issues in controlling the direct-drive arm: low damping, significance of link interaction, and nonlinear terms in arm dynamics.

The experiments in control of the direct-drive arm have demonstrated the solutions of the control issues, usefulness of employing a precise mathematical model into control, and the resultant excellent performance of the direct drive arm. First, it was shown that a sufficient damping can be provided by velocity feedback using accurate measurement of velocity by means of high-precision shaft encoders. The transient

response of joints, after gain adjustment, proved a very fast motion of the arm: the 6-th joint has less than 60 ms of delay time for a step input, and even the largest joint (1st joint) has about 350 ms of delay time.

Second, the experiment was performed on feedforward compensation of gravity force, link interaction, and Coliolis and centrifugal force. A remarkable improvement in dynamical performance was observed. Significance of this experiment is that we have demonstrated usefulness of feedforward compensation by being able to precisely model the arm dynamics, which is one of the biggest advantages of the direct-drive arm.

Third, the steady-state characteristics were also measured. The positional repeatability with 0.02 to 0.003 degree in standard deviation was achieved. The measured servo stiffness was as high as that of the Stanford Manipulator.

Acknowledgements

We thank Edward C. Kurtz and Kasturi V. Rangan for their help in constructing the CMU DD Arm, and Neil M. Swartz, Regis M. Hoffman and Steven J. Clark for their programming support.

References

[1] Asada, H. and Kanade, T.
"Design of Direct-Drive Mechanical Arms".
ASME Journal on Dynamics Systems, Measurement and Control, 1982.

[2] Asada, H., Kanade, T. etal.
"Development of the CMU Direct-Drive Arm".
Technical Report, Robotics Institute, Carnegie-Mellon University, 1982 (in preparation).

[3] Book, W., Maizza-Neto, J.O., and Whitney, D.E..
"Feedback Control of Two Beam, Two Joint Systems with Distributed Flexibility".
ASME Journal of Dynamic Systems, Measurement, and Control 97(4), December, 1975.

[4] Denavit, J., and Hartenberg, R.S.
"A Kinematic Notation for Lower Pair Mechanisms Based on Matrices".
ASME Journal of Applied Mechanics :215-221, June, 1955.

[5] Dubowsky, S., and DesForges, D.T.
"The Application of Model-Referenced Adaptive Control to Robot Manipulators".
ASME Journal of Dynamic Systems, Measurement, and Control 101(3):193-200, September, 1979.

[6] Hollerbach, J.M.
"A Recursive Lagrangian Formulation of Manipulator Dynamics and a Comparative Study of Dynamics Formulation Complexity .
IEEE Transaction on System, Man, and Cybernetics SMC-10(11), November, 1980.

[7] Horowitz, R., and Tomizuka, M.
"An Adaptive Control Scheme for Mechanical Manipulators - Compensation of Nonlinearity and Decoupling Control".
ASME Journal of Dynamic Systems, Measurement, and Control, 1981.

[8] Kasturi, R.
"Position and Velocity Measurement by Optical Shaft Encoders".
Technical Report, Robotics Institute, Carnegie-Mellon University, June, 1982 (to appear).

[9] LeBorgne, M., Ibarra, J. M., and Espiau, B.
"Adaptive Control of High Velocity Manipulators".
In *Proceedings of the 11-th Int. Symposium on Industrial Robots*, pages 227-236. Oct., 1981.

[10] Luh, J.Y.S., Walker, M.W., and Paul, R.P.C.
"On-Line Computational Scheme for Mechanical Manipulators".
ASME Journal of Dynamic Systems, Measurement, and Control 102(2):69-76, 1980.

[11] Paul, R.P.
"Robot Manipulators: Mathematics, Programming, and Control".
M.I.T. Press, 1981.

[12] Raibert, M.H., and Horn, B.H.K.
"Configuration Space Control".
The Industrial Robot :66-73, 1978.

[13] Stepanenko, Y., and Vukobratovic, M.
"Dynamics of Articulated Open-Chain Active Mechanisms".
Math. Biosci. 28:137-170, 1976.

[14] Takegaki, M., and Arimoto, S.
"An Adaptive Trajectory Control of Manipulators".
Int. Journal of Control 34(2):193-200, September, 1979.

[15] Vukobratovic, K.M., and Stokic, D.M.
"Contribution to the Decoupled Control of Large-Scale Mechanical Systems".
Automatica, January, 1980.

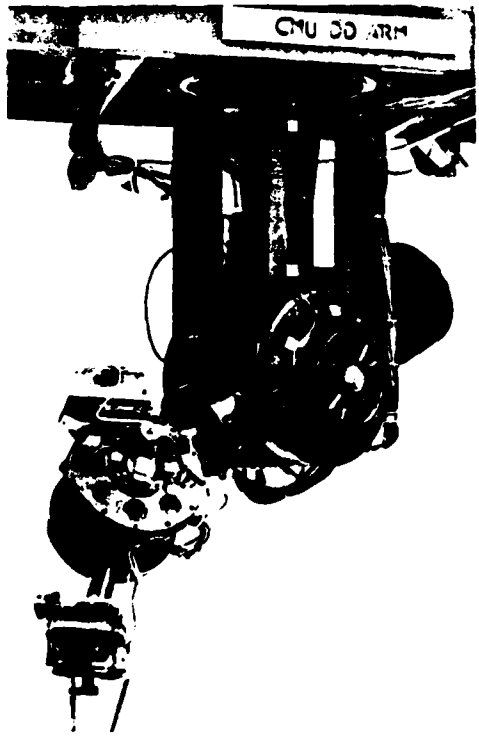

Photo 1 Overall view of direct-drive arm

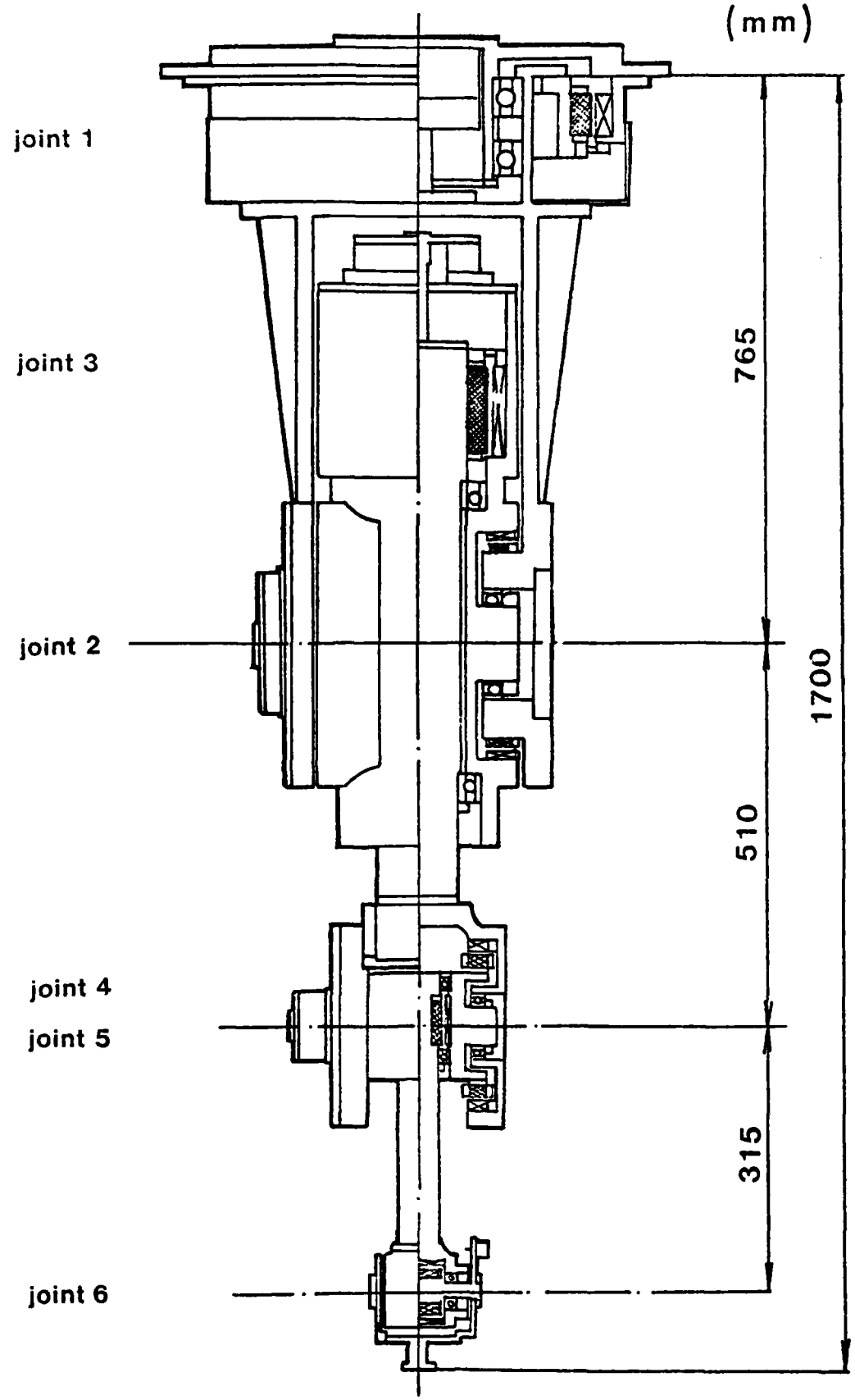

Figure 1: Drawing of CMU Direct-Drive Arm

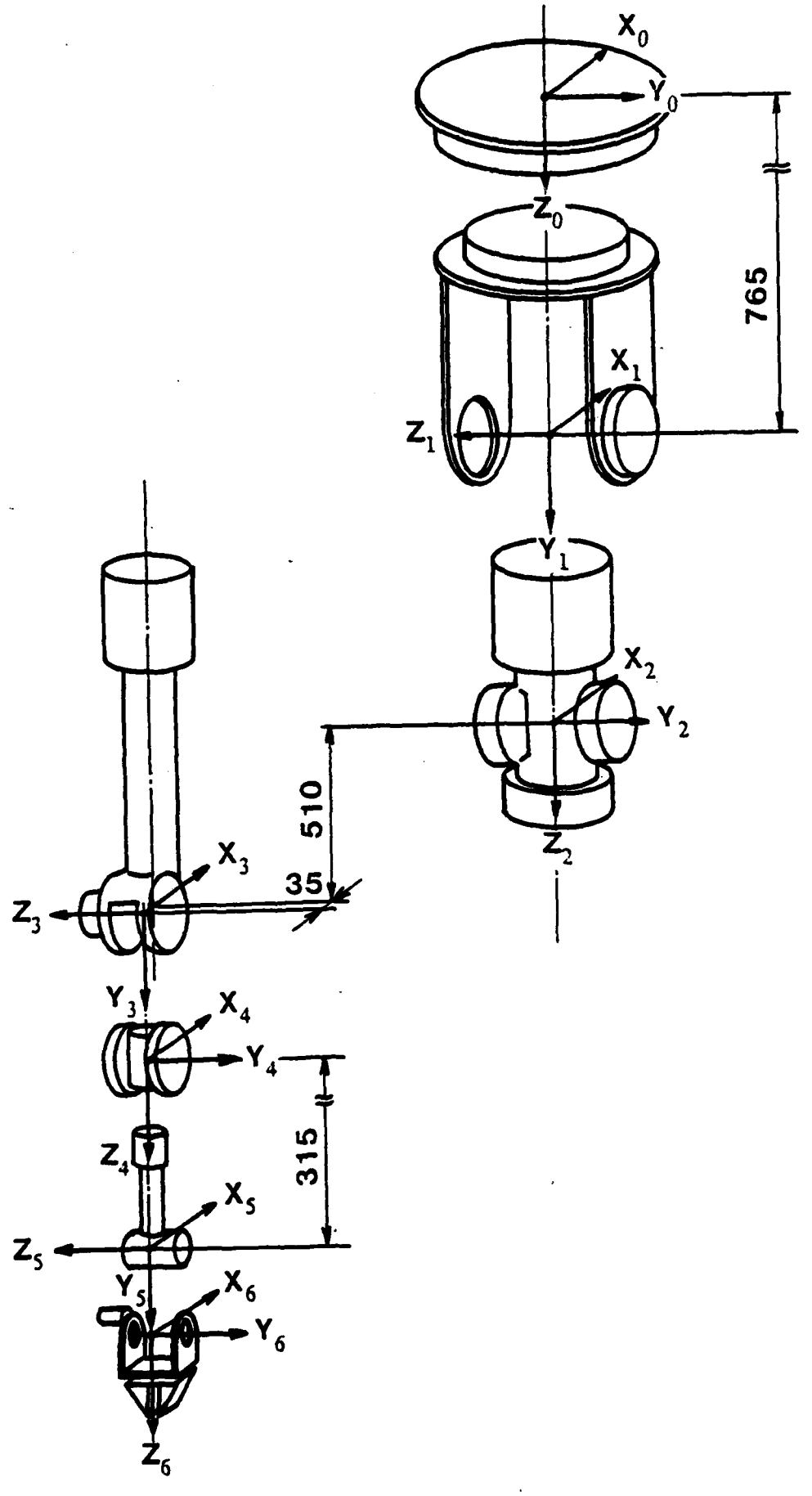

Figure 2: Disconnected links

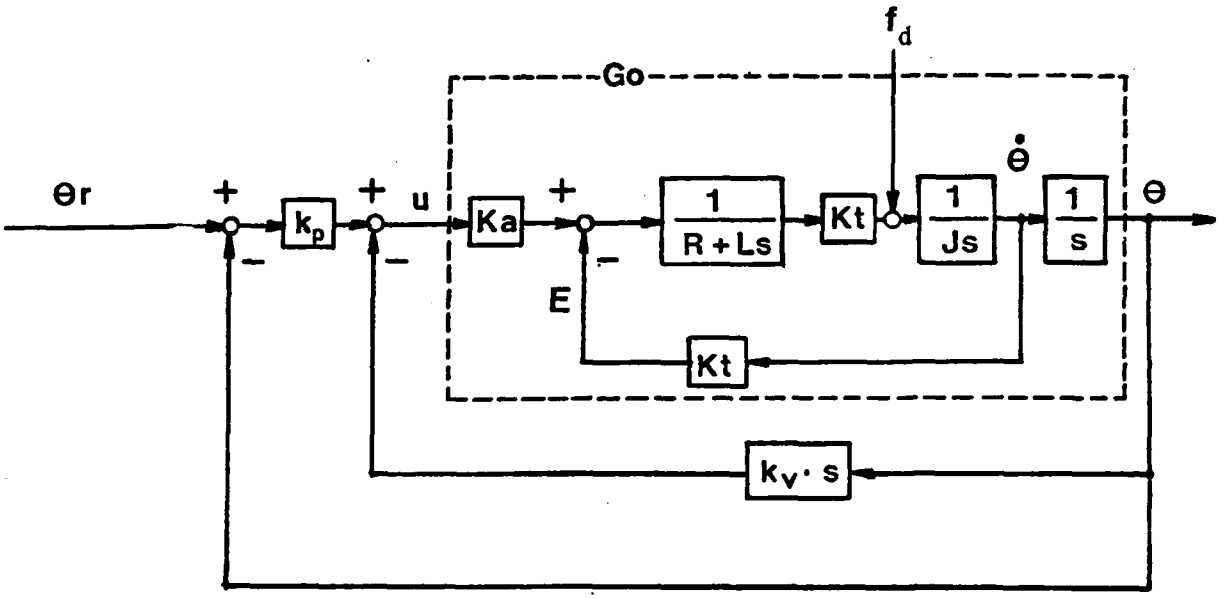

Figure 3: Block diagram of single-link drive system

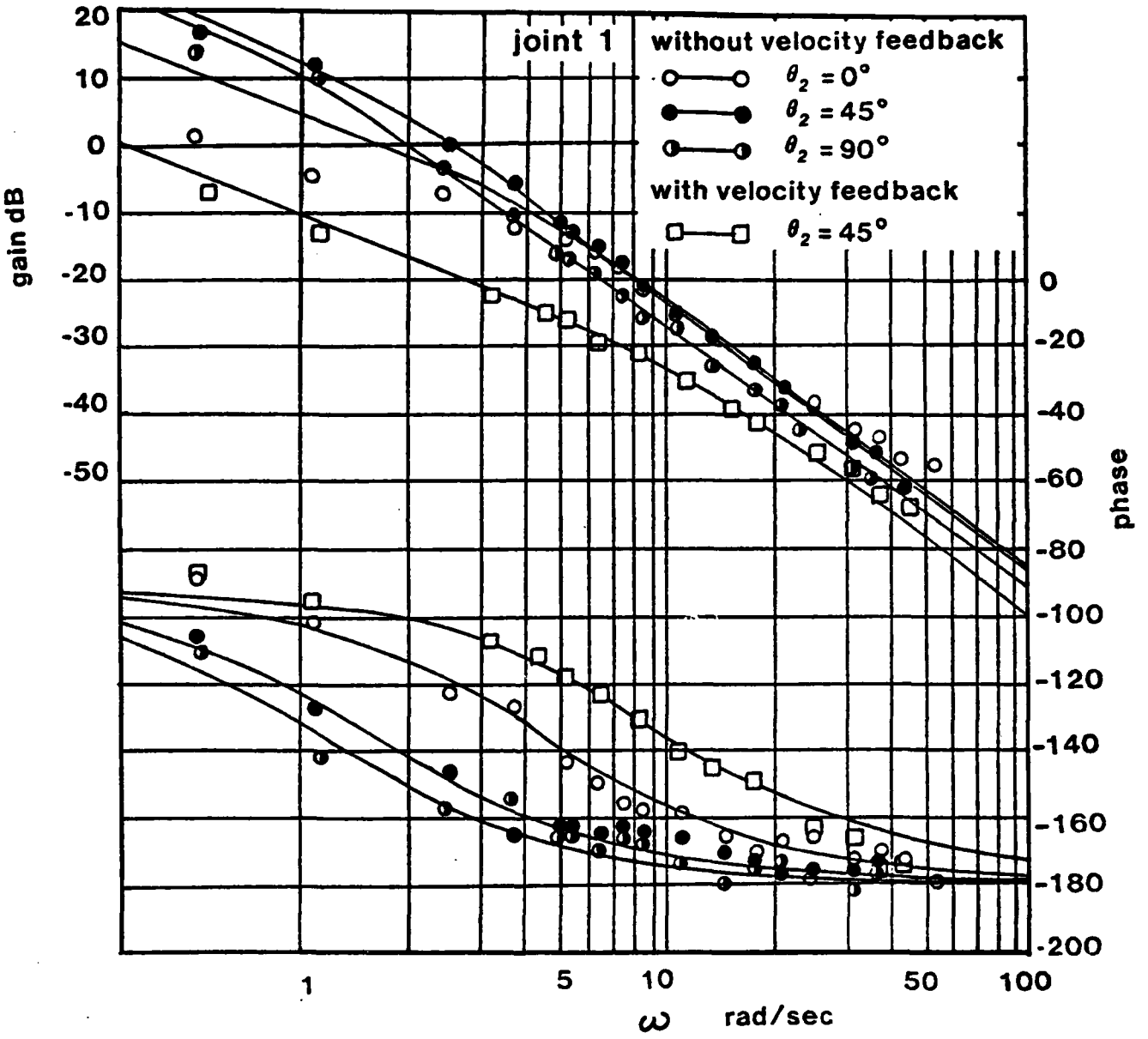

Figure 4: Frequency response of joint 1 with various arm configurations

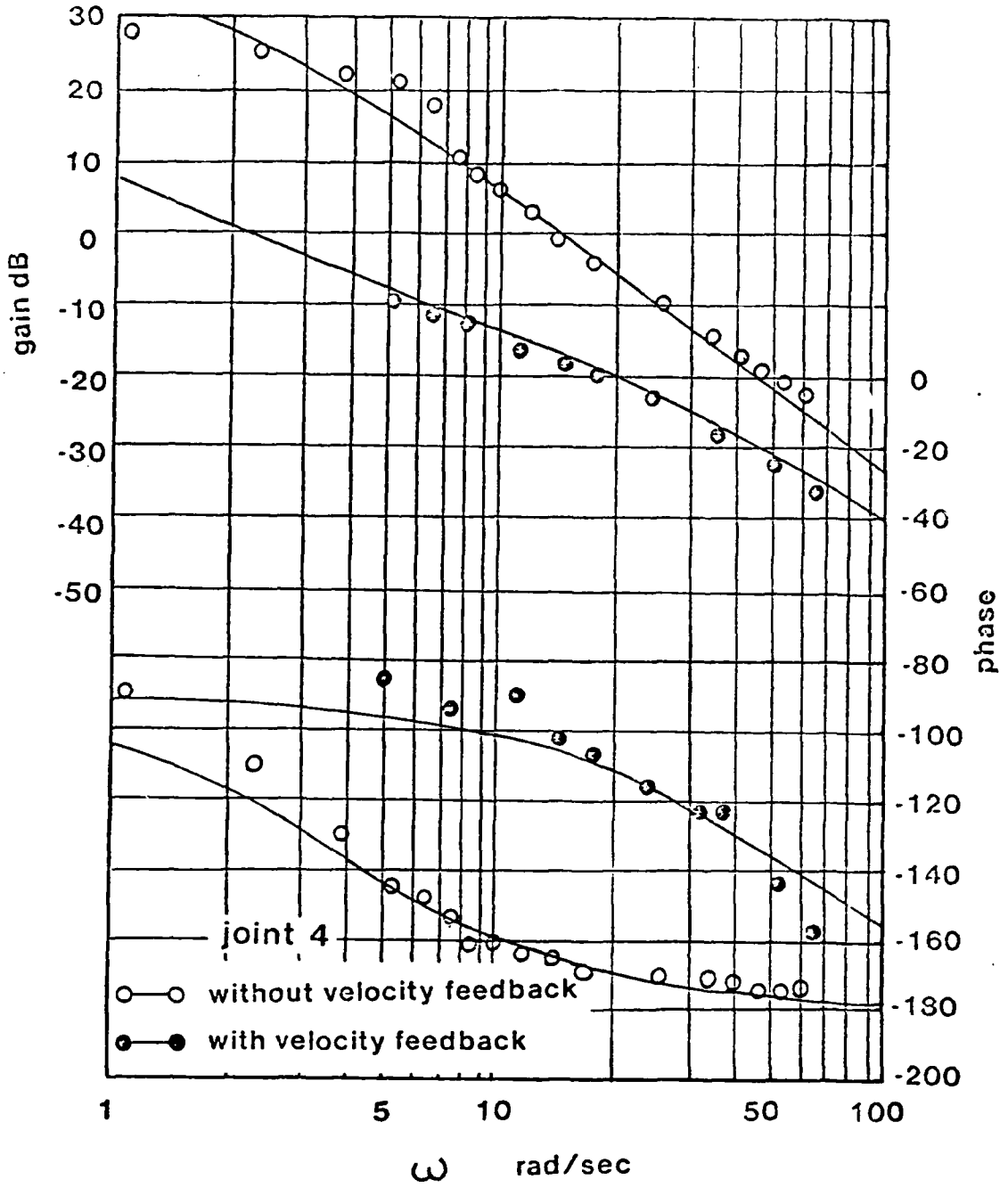

Figure 5: frequency response of joint 4

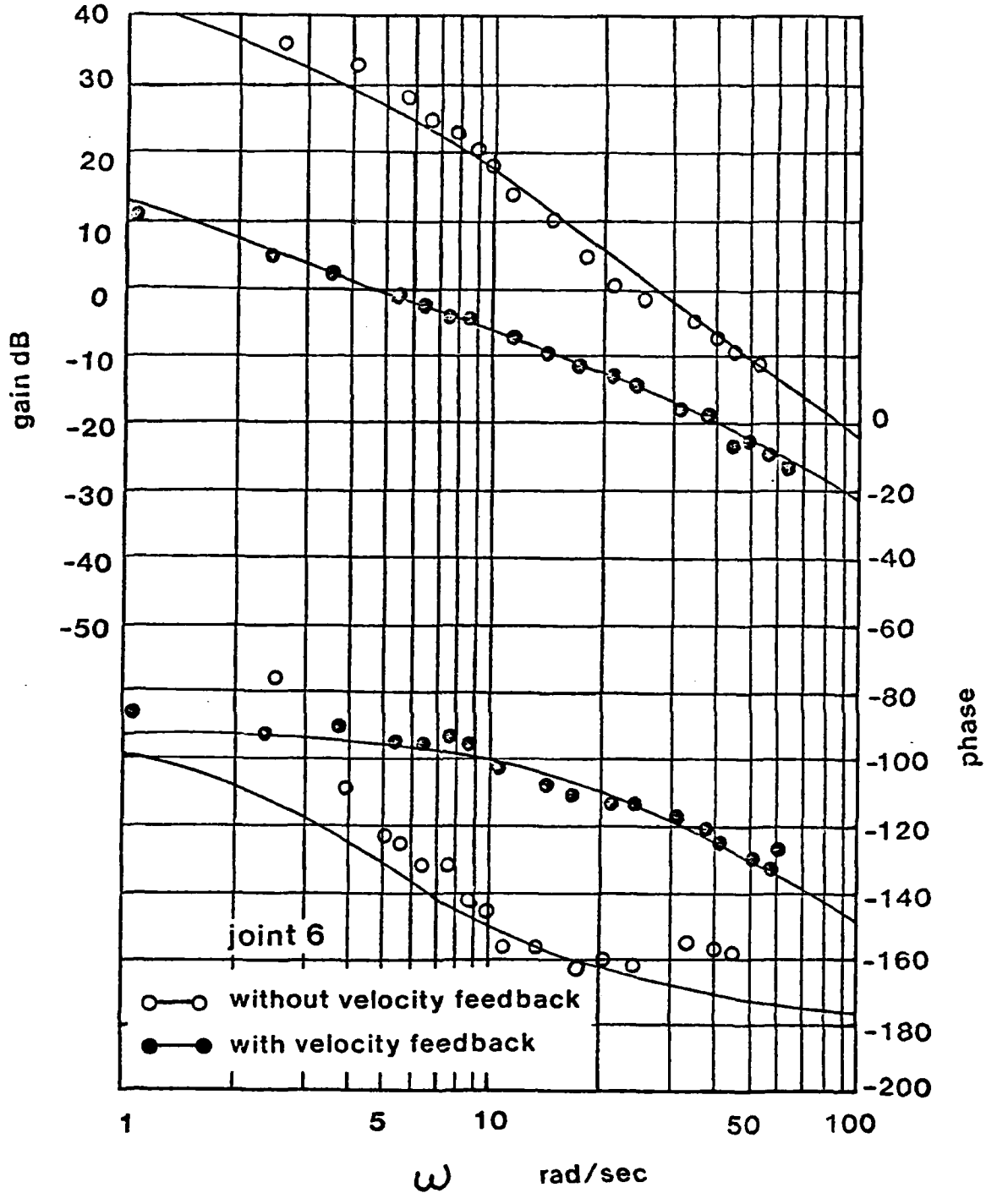

Figure 6: Frequency response of joint 6

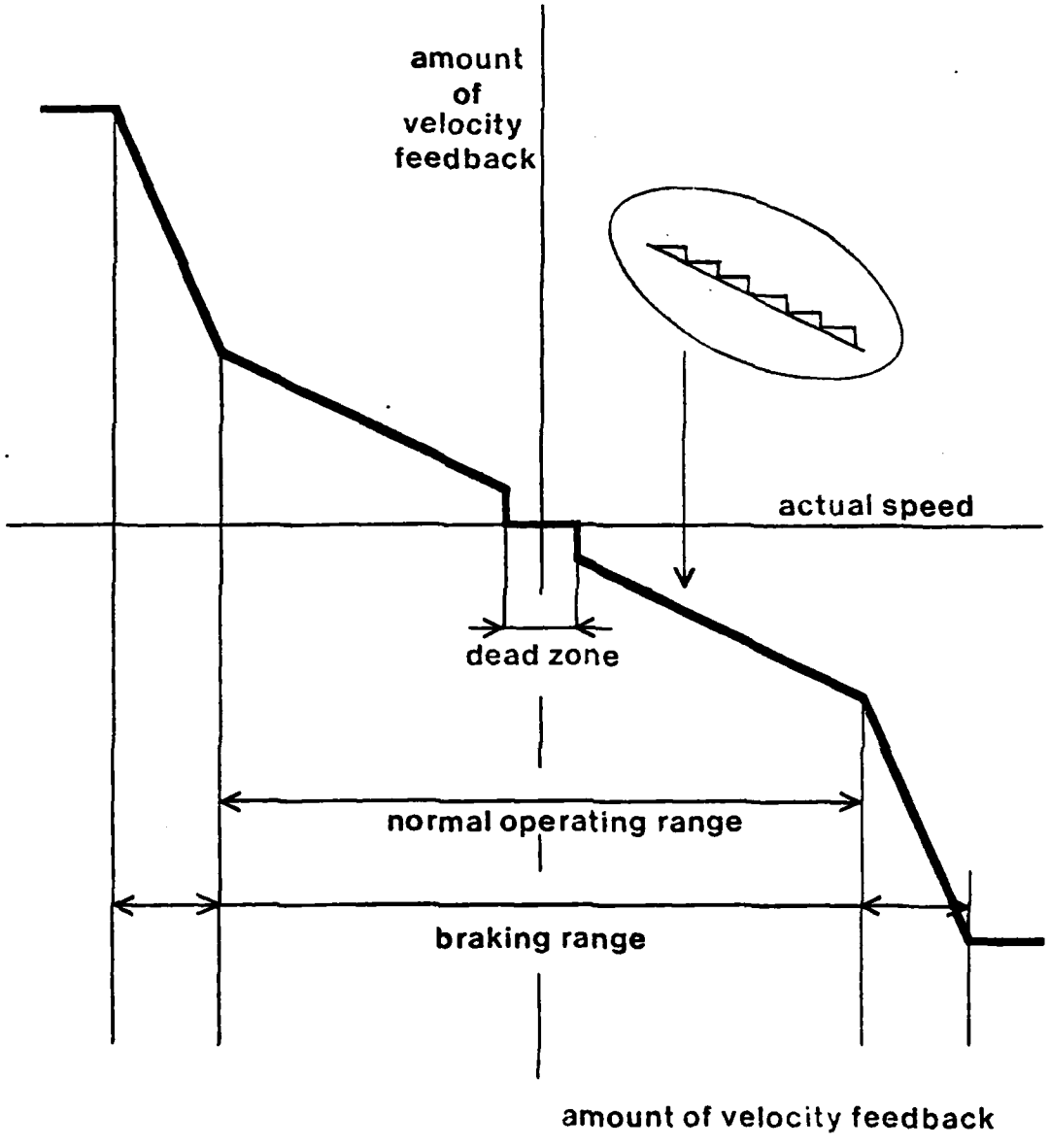

Figure 7: Characteristics of velocity measurement

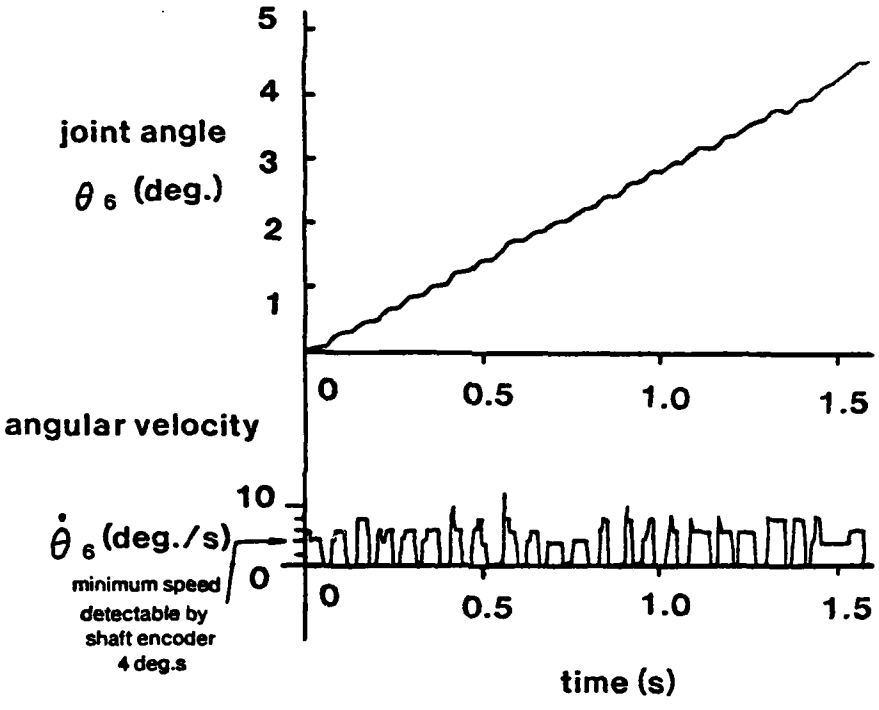

Figure 8: Vibration in slow speed

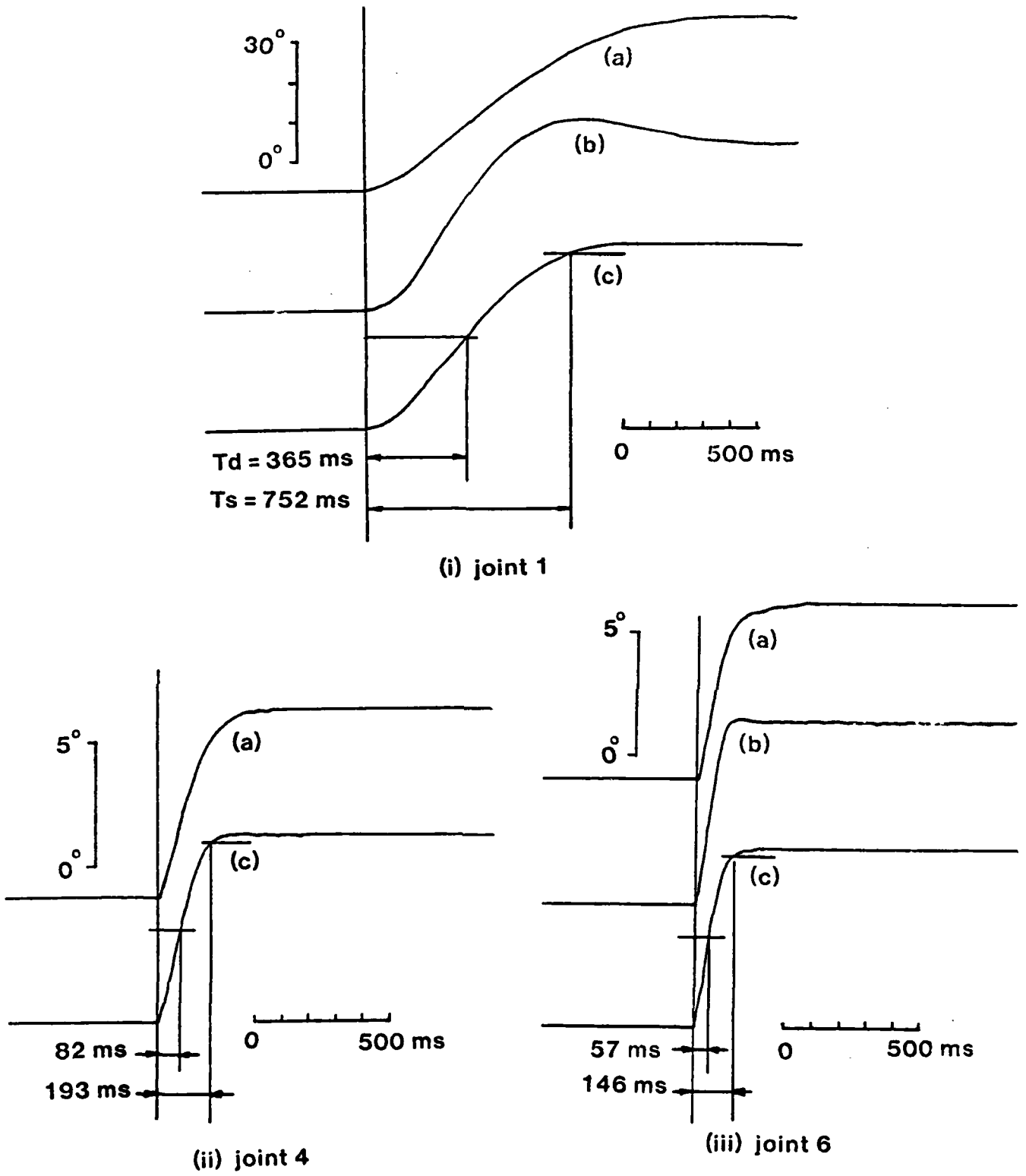

Figure 9: Experiment of step response

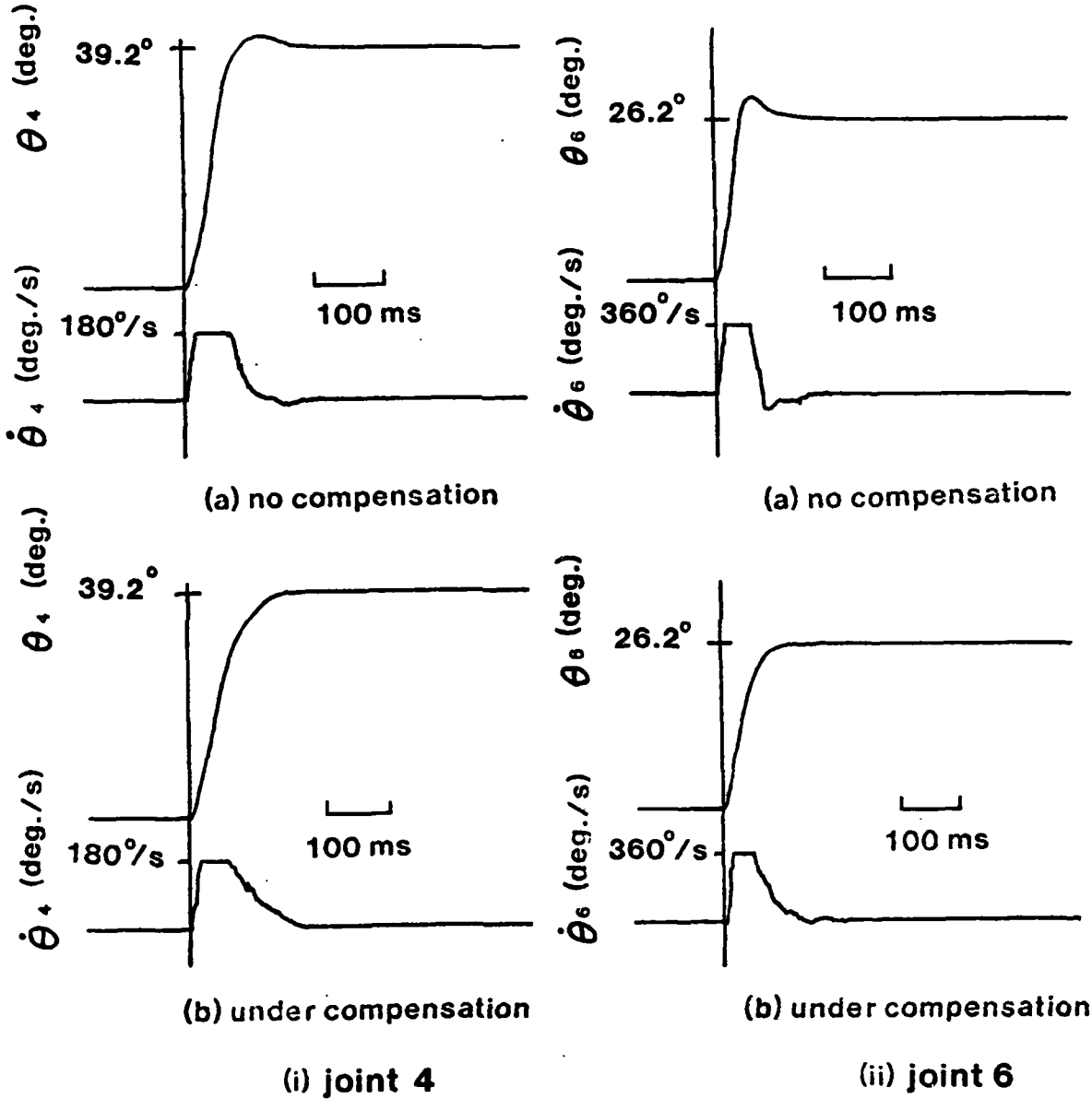

Figure 10: Effect of compensation for saturation of velocity measuring circuit

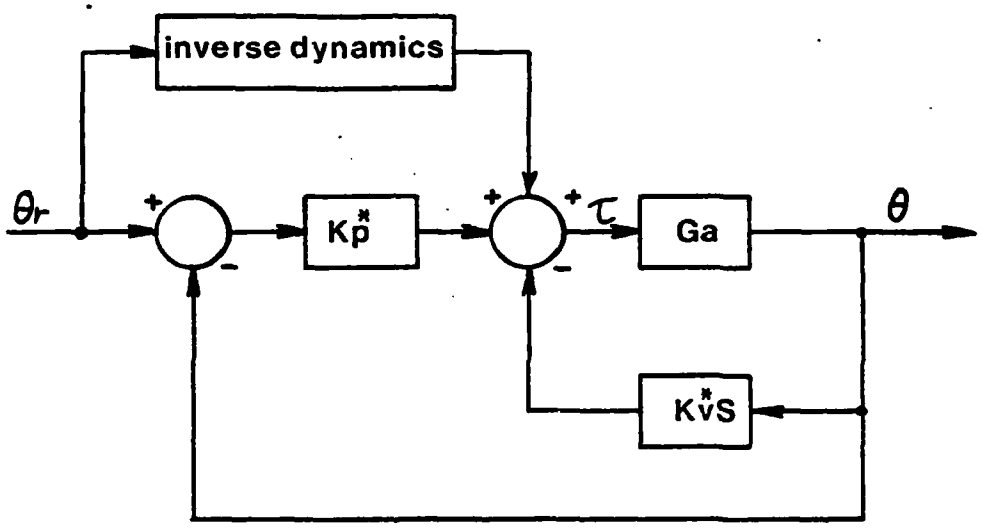

Figure 11: Feedback and feedforward compensation

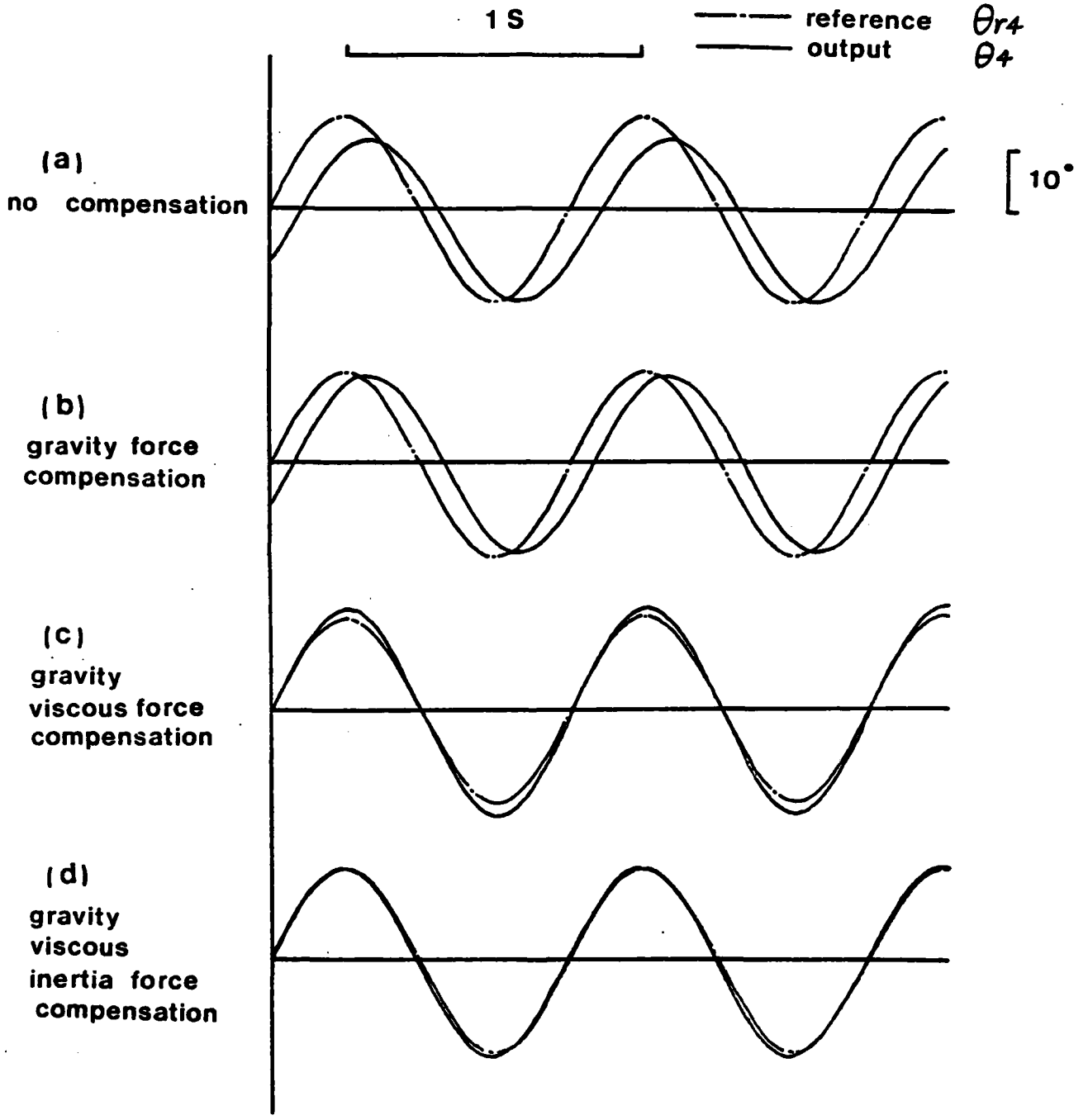

Figure 12: Effect of feedforward compensation: case of a single joint

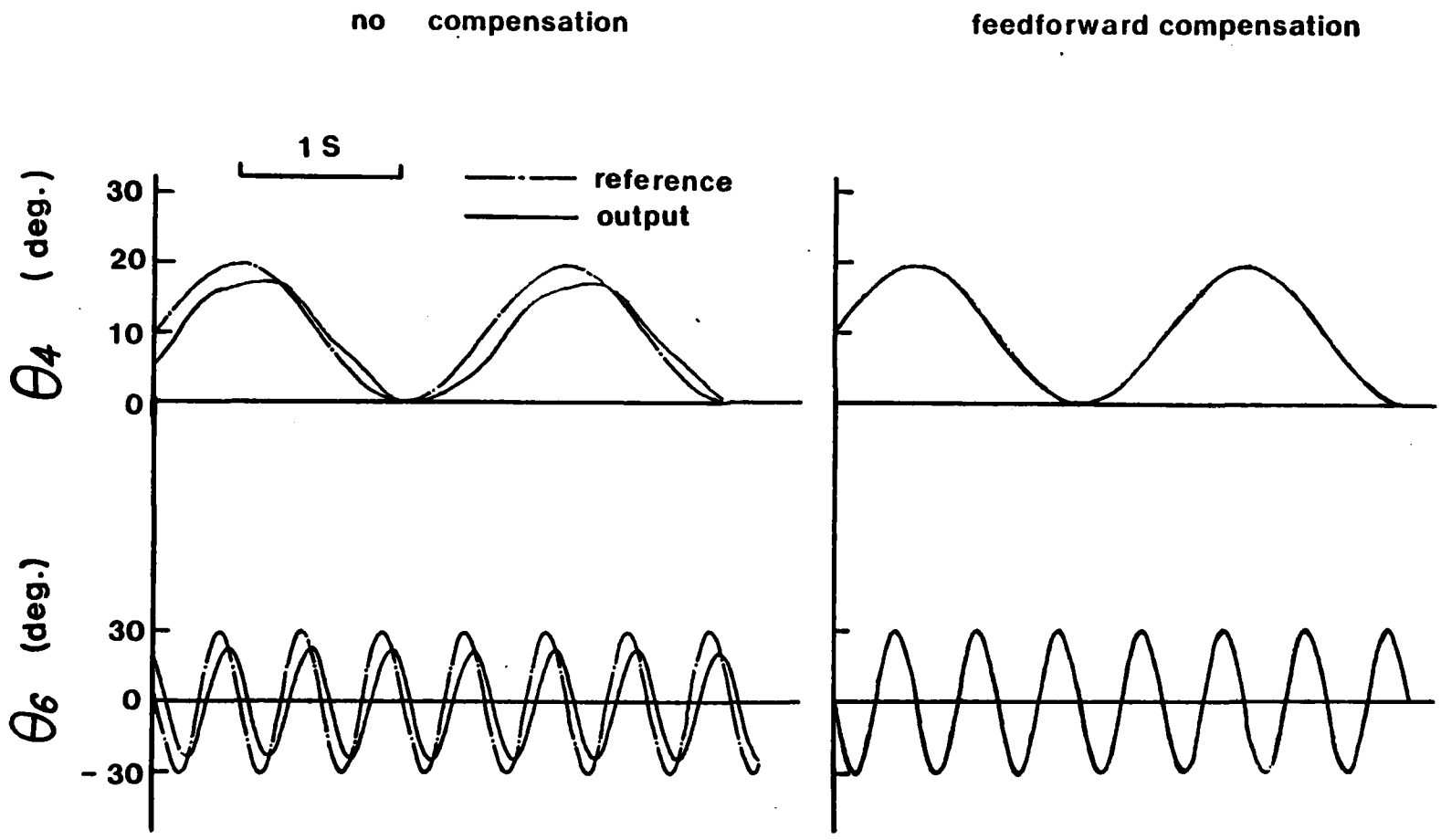

Figure 13: Effect of feedforward compensation: case of multiple joints with interacion

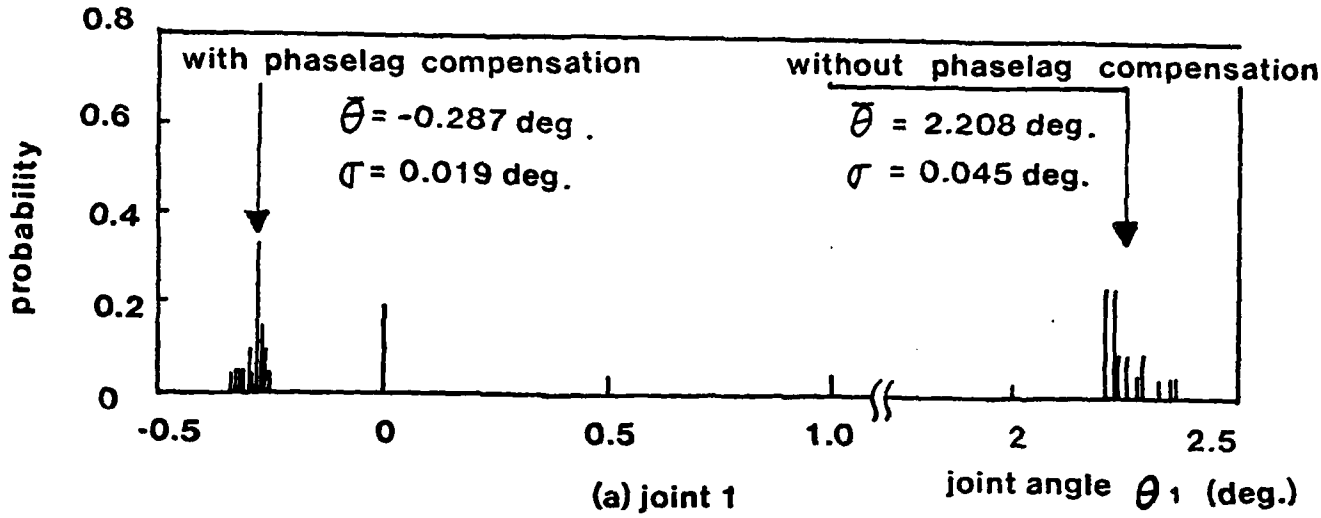

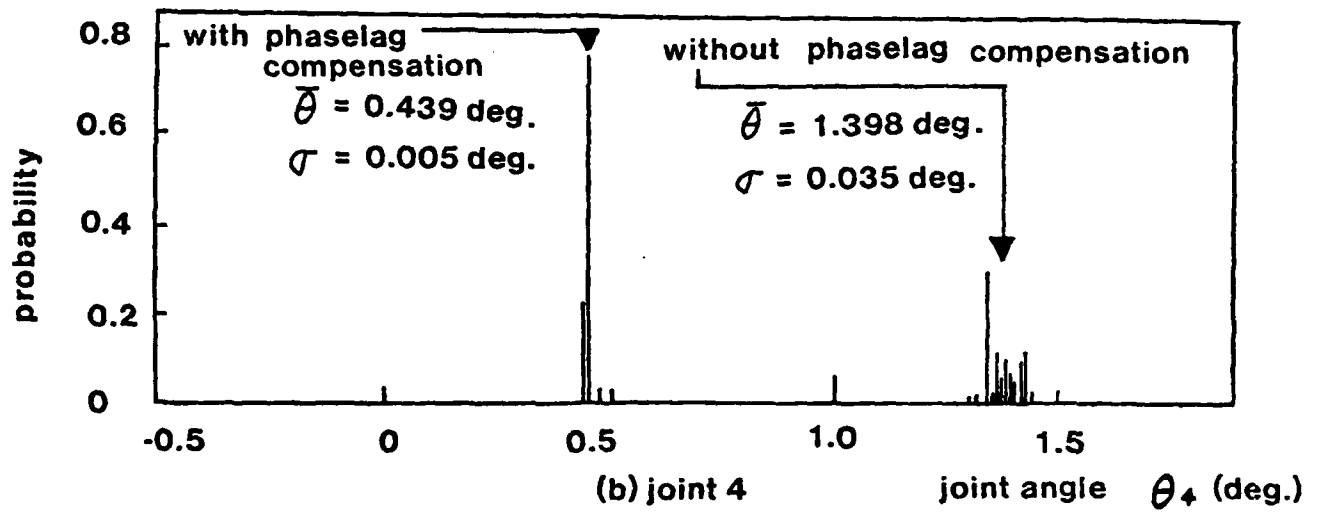

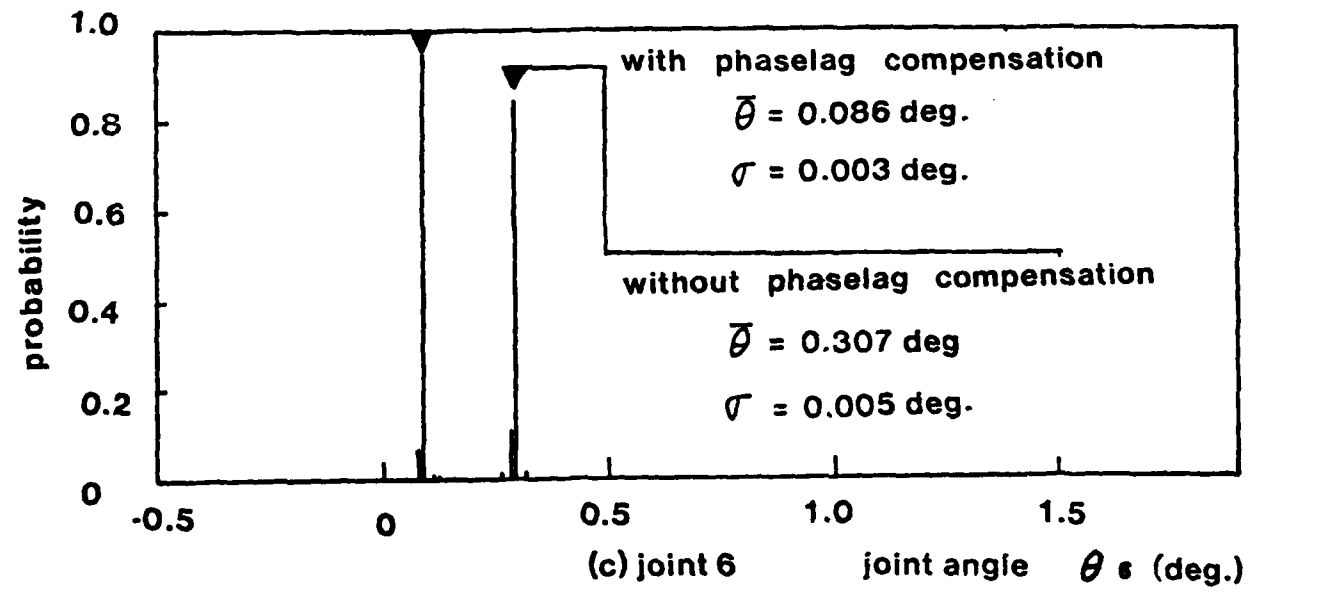

Figure 14: Positional repeatability

Table 1: Description of the kinematics of CMU DDArm

in Denavit-Hartenberg convention

joint #	s_i (m)	a_i (m)	α_i (deg.)
1	0.765	0	90
2	0	0	-90
3	0.510	-0.035	90
4	0	0	-90
5	0.315	0	90
6	0	0	-90

Table 2: Mass and moment of inertia of CMU DDArm

link number	mass (kg) m	center of mass (m) p	moment of inertia (kgm^2) I_{link}		
		0.000	33.724	0.000	0.000
1	95.99	-0.675	0.000	2.879	0.609
		-0.015	0.000	0.609	33.056
		0.000	3.990	0.000	0.001
2	82.61	0.010	0.000	3.786	-0.154
		-0.203	0.001	-0.154	1.475
		0.029	8.295	0.178	-0.012
3	52.90	-0.524	0.178	0.425	0.195
		-0.007	-0.012	0.195	8.237
		-0.001	0.150	0.000	-0.001
4	13.34	0.024	0.000	0.062	0.001
		0.002	-0.001	0.001	0.150
		0.002	0.110	-0.002	0.000
5	4.84	-0.176	-0.002	0.005	0.000
		0.000	0.000	0.000	0.110
		0.000	0.016	0.000	0.000
6	2.81	0.008	0.000	0.011	0.002
		0.032	0.000	0.002	0.006

Table 3: Identified parameters of actuators

joint #		torque constant Kt (Nm/A)	gain of servo amplifier Ka	armature resistance R (Ω)	damping coefficient C (NmS/rad)	torque gain K (Nm/V)
1		6.25	5.46	2.15	18.17	15.88
2	motor1	4.19	5.40	2.80	12.28	15.83
	motor2	4.19	5.40	2.92		
3		2.42	5.45	2.29	2.56	5.76
4	motor1	1.67	4.86	2.15	2.31	7.15
	motor2	1.53	5.08	2.30		
5		1.14	11.65	9.78	0.133	1.36
6		1.16	16.85	9.10	0.148	2.15

Table 4: Time constants and improvement of dynamic characteristics by velocity feedback

joint #	time constant of open-loop system T (S)	maximum allowable velocity feedback gain Kv (rad/SV)	time constant under velocity feedback T (S)
1	0.585	4.89	0.092
4	0.269	2.45	0.019
6	0.181	0.98	0.017

Table 5: Servo stiffness

joint #	length l(mm)	servo stiffness without compensation Ks (N/mm)	servo stiffness with compensation Ks (N/mm)
1	510	0.32	3.2
4	315	1.06	10.6
6	110	2.88	28.8

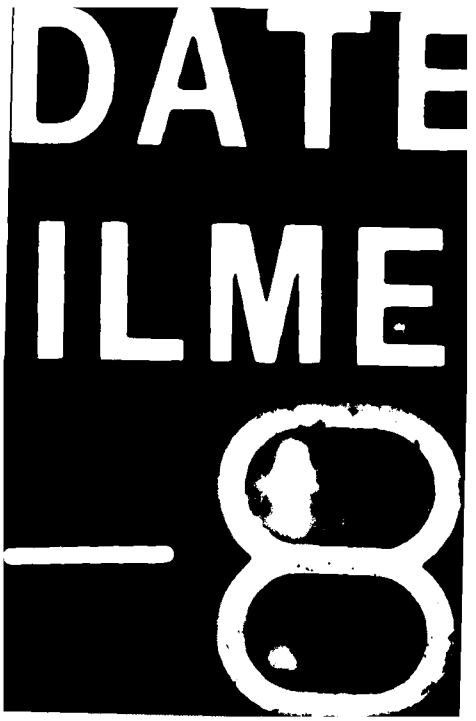
DATE
ILME
8